



**HAL**  
open science

## Photonic crystal backbone for light trapping inside an ultrathin, low absorbing layer

Said El-Jallal, Marion Hochedel, Jérôme Capitolis, Hai Son Nguyen, Céline Chevalier, Jean -Louis Leclercq, Mohamed Amara, Christian Seassal, Emmanuel Drouard

► **To cite this version:**

Said El-Jallal, Marion Hochedel, Jérôme Capitolis, Hai Son Nguyen, Céline Chevalier, et al.. Photonic crystal backbone for light trapping inside an ultrathin, low absorbing layer. *Optics Express*, 2022, 30 (16), pp.29694. 10.1364/OE.461390 . hal-03766724

**HAL Id: hal-03766724**

**<https://hal.science/hal-03766724v1>**

Submitted on 22 Nov 2022

**HAL** is a multi-disciplinary open access archive for the deposit and dissemination of scientific research documents, whether they are published or not. The documents may come from teaching and research institutions in France or abroad, or from public or private research centers.

L'archive ouverte pluridisciplinaire **HAL**, est destinée au dépôt et à la diffusion de documents scientifiques de niveau recherche, publiés ou non, émanant des établissements d'enseignement et de recherche français ou étrangers, des laboratoires publics ou privés.



# Photonic crystal backbone for light trapping inside an ultrathin, low absorbing layer

SAID EL-JALLAL,<sup>1,2,4</sup> MARION HOCHEDÉL,<sup>1</sup> JÉRÔME CAPITOLIS,<sup>1</sup>  
HAI-SON NGUYEN,<sup>1,3</sup> CÉLINE CHEVALIER,<sup>1</sup> JEAN-LOUIS  
LECLERCQ,<sup>1</sup> MOHAMED AMARA,<sup>1</sup> CHRISTIAN SEASSAL,<sup>1</sup> AND  
EMMANUEL DROUARD<sup>1,\*</sup> 

<sup>1</sup>Univ. Lyon, CNRS, Ecole Centrale de Lyon, INSA Lyon, Université Claude Bernard Lyon 1, CPE Lyon, INL, UMR5270, 69134 Ecully, France

<sup>2</sup>Univ. Cadi Ayyad, Ecole Normale Supérieure, LIRBEM, BP 2400, 40000 Marrakech, Morocco

<sup>3</sup>Institut Universitaire de France, MESRI, 75231 Paris, France

<sup>4</sup>s.el-jallal@uca.ma

\*emmanuel.drouard@ec-lyon.fr

**Abstract:** A few tens of nanometre thick ultrathin materials may suffer from a very low absorption at their band edges. In this work, we investigate a photonic crystal (PC) made of a lowcost, transparent patterned silicon nitride (SiN<sub>x</sub>) layer, conformally covered with an ultrathin active layer (e.g., 20 nm TiO<sub>2</sub>) in view of its use in various applications such as photocatalysis. A fair estimation of the absorption enhancement, considering the volume of the active material, is calculated using RCWA. A remarkable enhancement (more than ten-folds) in absorptance in the near UV range and a very high transmittance over the visible range are observed. A detailed modal analysis of the structures-of-interest unravels the Light Trapping (LT) mechanisms and allows the derivation of key design guidelines. Optical measurements on a patterned sample provide a first proof-of-concept of such possible photonic backbone structures suitable for highly efficient depollution and artificial photosynthesis for solar fuels production.

© 2022 Optica Publishing Group under the terms of the [Optica Open Access Publishing Agreement](#)

## 1. Introduction

Photonic crystals (PCs) have been extensively used for light trapping (LT) in energy harvesting applications, such as in thin film photovoltaics [1] and more recently in photo catalysis [2,3], especially with inverse opals [4,5]. LT results from the resonant diffractive coupling of the impinging light into the guided modes of the sample. It constitutes the most efficient approach to enhance the absorption in poorly absorbing films.

One particularly interesting implementation consists of a high index transparent film structured as a PC with an optical thickness in the same order of the wavelength. The film acts as a backbone and is then conformally coated with an active ultrathin layer of a low absorption material [6]. Such an heterogeneous photonic structure has been proposed to enhance the wavelength conversion in lanthanide ions-doped media, for either frequency down- [7] or up-conversion [8–10], using periodic backbones. Thus, the PC can be realized by the means of rather simple, scalable top down approaches, while enabling a strong enhancement of the light matter interaction in the active layer coating.

In this study, we focus on TiO<sub>2</sub>, which is a low cost material widely used in photo catalysis. The excitation energy is used to generate electron-holes pairs leading to chemical reactions, which can be used for photosynthesis or depollution [11].

Nevertheless, TiO<sub>2</sub> has a limited absorption in the near UV range (more precisely the so-called “A1” UV range) due to its band-gap energy of 3.25 eV, especially when thin layers (i.e. 20 nm) are used to limit the photo carriers’ recombination occurring in thicker media.

Thus, we consider a non-stoichiometric, UV-transparent, silicon nitride ( $\text{SiN}_x$ ) film ( $\sim 200$  nm thick) regularly patterned, as the backbone. This is intended to enhance the absorption in  $\text{TiO}_2$  in the near UV range, while being almost transparent at least in the visible range.

A photonic crystal (PC) commonly consists of a square or triangular lattice of low index media, such as partially etched holes, incorporated into a high index material. However, in the case of a PC based on a lattice of high index pillars laying in an air or liquid medium, the flow circulation around and through the lattice becomes much easier. **Figure 1** illustrates an example of this structure.

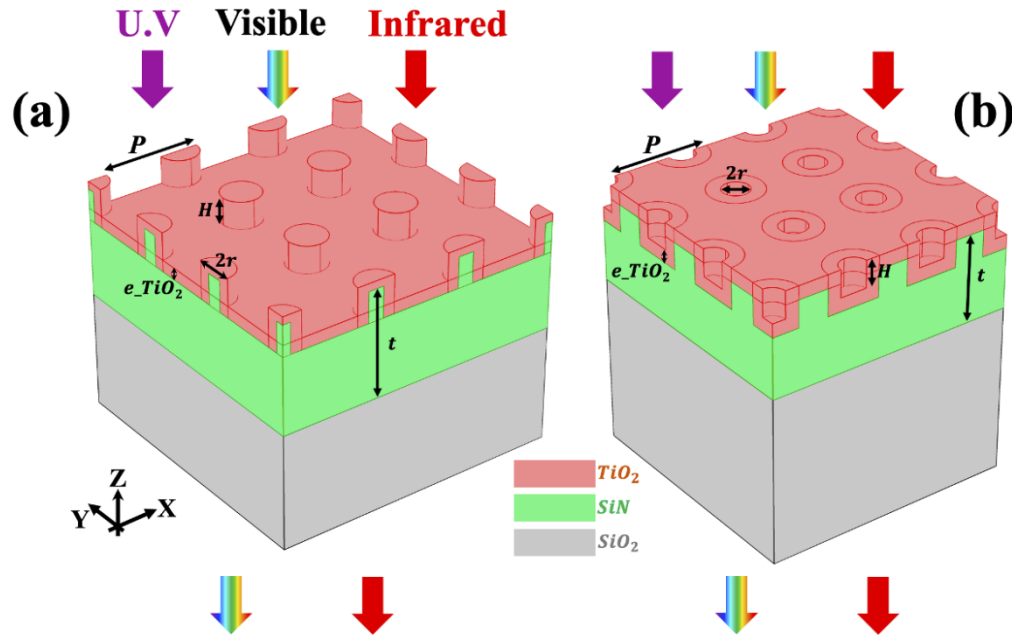


**Fig. 1.** (a) Pillar-array structure, (b) Backbone with holes geometry: pillars and holes radii ( $r$ ), pillar height ( $H_p$ ), holes depth ( $H$ ), SiN thickness ( $t$ ).

In this study, we are mainly interested in the detailed optical analysis of this backbone structure with the aim of maximizing the absorption of the  $\text{TiO}_2$  coating layer in the near UV range. Our goal consists in establishing key guidelines for the backbone design, focusing on the integrated absorbance per unit area of the active material compared to the one of a flat reference, which is considered as a key parameter for improving the structure performance. The normalized integrated absorbance per unit area enables the estimation of the real light trapping (LT) impact, while changing the geometrical parameters of the PC. It helps eliminating the effect of simply increasing the volume of the active material.

We also intend to provide a comprehensive analysis of the absorbance enhancement caused by the PC backbone. For this, the arising of Bloch resonances in such structures is described using a phenomenological approach, based on our previous work in a similar case [12]. It will be shown that only selected Bloch resonances, deriving from optimal values of the backbone thickness and lattice parameter, can lead to optimized absorbance.

The remaining of the paper is organized as follows. The detailed presentation of the structure and design methodology are described in section 2. Simulation results are presented and analyzed in section 3. Section 4 is devoted to the experimental results (fabrication and characterization), and section 5 summarizes the conclusions of this work.

## 2. General design of the backbone structure and methodology

### 2.1. Geometrical properties of the structures

The designed photonic structures are made of an ultrathin TiO<sub>2</sub> layer coating the surface of a patterned SiN<sub>x</sub> layer (the backbone), the whole lying on a SiO<sub>2</sub> substrate. Practically, such a conformal coating can be obtained using Atomic Layer Deposition (ALD). The incidence medium is chosen to be mainly air, but the case of water is also envisaged.

Given the fully negligible absorption of TiO<sub>2</sub> at larger wavelengths (see indices in **Fig. S1**), the absorption range on this study is the near UV, starting from 340 up to 375 nm. The SiN<sub>x</sub> film considered here (see indices in **Fig. S2**) is transparent over the whole investigated wavelength range, and its thickness  $t$  (before structuring) was set between 200 nm and 290 nm. A preliminary study has shown that such a slab exhibits at least two guided modes in each polarisation state that could contribute to the LT. At the wavelength  $\lambda = 360$  nm, the lowest order mode ( $m = 0$ ) has an effective index  $n_{eff,0} \sim 1.8$ , whereas the highest order mode ( $m = 1$ ) has an effective index  $n_{eff,1} \sim 1.6$  (see Table S1). Thus, according to a simple perturbative approach based on 1D grating equation (further developed in section 2.3), the period (lattice parameter)  $P$  should be on the order of  $\lambda/n_{eff}$ . It turns out that  $P$  values in the range 200 to 250 nm should lead to the efficient 1<sup>st</sup> order diffraction of these two first guided modes in the near UV range.

We have considered two types of backbones, both arranged in a square lattice. The first one consists in circular holes etched in SiN<sub>x</sub>, whereas the second one consists in cylindrical SiN<sub>x</sub> pillars (**Fig. 1**). The holes or pillars radii and the etching depth were adjusted using lithography and etching processes. The TiO<sub>2</sub> layer is supposed to be conformally deposited with a thickness of 20 nm.

The air filling fraction  $aff$  is a meaningful estimation of the perturbation for the unpatterned stack. For holes, it is defined as:

$$aff = \frac{\pi r^2}{P^2}, \quad (1)$$

where  $r$  is the radius of the air hole after coating by the 20 nm thick TiO<sub>2</sub>. For pillars

$$aff = 1 - \frac{\pi r^2}{P^2} \quad (2)$$

where  $r$  is the outside radius of the 20 nm thick TiO<sub>2</sub> tube resulting from the lateral conformal coating of the SiN<sub>x</sub> pillars. Thus, the surface of TiO<sub>2</sub> is given by:

$$S_{TiO_2} = 2\pi rH + P^2, \quad (3)$$

where  $P$  is the lattice parameter and  $H$  is the depth of the hole or the height of the pillar.

Equation (3) indicates that the surface of TiO<sub>2</sub> increases with all parameters, and so does the volume, due to the constant thickness of the conformal TiO<sub>2</sub>. It is thus of primary importance to normalize the integrated absorptance to unravel the possible LT effects.

All geometrical parameters have been considered within ranges that are either derived from given previous preliminary considerations on guided modes of interest (especially  $t$ ), or that are achievable using lithography techniques compatible with large surfaces and usual etching techniques, as detailed later. The parameters and corresponding ranges are summarized in **Table 1**. For each parameter (including the radius), the sampling step is set to 10 nm, to take into account the limited accuracy of the fabrication techniques.

### 2.2. Electromagnetic simulation and absorptance enhancement calculation methods

All numerical simulations presented in this paper were performed using the Rigorous Coupled Wave Analysis (RCWA) [13] with the S<sup>4</sup> distribution [14]. These simulations provide the spectral reflectance  $R(\lambda)$  and transmittance  $T(\lambda)$  of the structure, under normal incidence. As TiO<sub>2</sub> is

**Table 1. Maximum and minimum values for all geometrical parameters**

Parameters	Min limit	Max limit
Period $P$ (nm)	200	250
Air filling factor $aff$ (%)	holes	7
	pillars	30
Height of the patterns $H$ (nm)	80	140
SiN <sub>x</sub> thickness $t$ (nm)	200	290
Wavelength $\lambda$ (nm)	340	375

the only absorbing material in the spectral domain of interest, its spectral absorptance is simply  $A(\lambda) = 1 - R(\lambda) - T(\lambda)$ .

For any given structure of spectral absorptance  $A(\lambda)$ , the integrated absorptance  $A_{int}$  is given by:

$$A_{int} = \frac{\int_{\lambda_{min}}^{\lambda_{max}} A(\lambda) d\lambda}{\Delta\lambda}, \quad (4)$$

where  $\Delta\lambda = \lambda_{max} - \lambda_{min}$ .

The absorptance of each sample has to be divided by the TiO<sub>2</sub> surface of the given sample for further comparison between patterned structures.

Finally, the enhancement of the integrated absorptance per unit area,  $\xi$ , for a given patterned structure is defined as:

$$\xi = \frac{A_{int}}{A_{int,ref}} \frac{P^2}{S_{TiO_2}}, \quad (5)$$

where  $A_{int,ref}$  is the integrated absorptance of the unit area of the planar stack considered as a reference.

### 2.3. Basics on LT in PC membranes

Light trapping in PC membranes has been studied for solar energy harvesting, especially in photovoltaics [15]. For instance, we recall some useful basics for the analysis of optimal structures arising from the numerical study. Further developments and justifications of this phenomenological approach can be found elsewhere in the slightly simpler, but similar case, of 1D patterned waveguides [12]. It is worth noting that the incoming light is usually considered as a plane wave under normal incidence.

To fully understand the Bloch modes implied in the light trapping phenomenon, examining simple  $A$  or  $R$  spectra is not sufficient, especially in case of degenerate modes leading to broad peaks in  $A(\lambda)$ . An energy-momentum band diagram is often required. If the in-plane wavevector can evolve only along one direction of the lattice, the spectral domain should be extended to the lowest energies, such as to include the lowest diffracted orders.

The band diagram of a PC could be roughly understood using phenomenological approaches. For a bulk homogenous medium, any small periodic patterning implies diffraction. The corresponding “free photon diagram” is obtained by a “band folding mechanism” at the edges of the first Brillouin zone [16]. Then, the photonic bandgap opening resulting from large index contrast could be described using the coupled mode theory.

Thus, according to the diffraction theory, in a hypothetical 2D PC (infinitely thick) square lattice, the 4 lowest energy modes under normal incidence ( $\Gamma$  point of the reciprocal space) for each polarisation state result from first order diffraction, i.e.  $(N_x, N_y) = (\pm 1, 0), (0, \pm 1)$ . Similarly the 4 modes of higher energy result from the second order diffraction, i.e.  $(N_x, N_y) = (\pm 1, \pm 1)$ , and so on.

In actual 2D PC membranes, the aforementioned diffraction mechanism remains true, but “free photon modes” become the guided modes of the membrane. This means that if the non-corrugated membrane supports several guided modes, then, each guided mode should lead to its own diffracted orders in each polarization state. Roughly speaking, the energy domain of every set of four Bloch modes for a given diffraction order increases as the effective index of the guided mode decreases. We recall that the Transverse Magnetic (TM) guided mode of a given order has a lower effective index than the one of the Transverse Electric (TE) guided mode of the same order ( $n_{eff\ TM, m} < n_{eff\ TE, m}$ ). However, considering overlaps of these energy domains (i.e. mode coupling), typically only four Bloch modes per guided mode order remain.

Moreover, in such membranes, some Bloch modes can couple to the plane waves of the free space, leading to Bloch resonances.

Thus, at normal incidence (so-called  $\Gamma$  point in the first Brillouin zone), two kinds of Bloch modes exist, which are commonly called the “dark” and “bright” modes. Due to spatially antisymmetric in-plane ( $x, y$ ) components of the electric field, the overlap with a plane wave under normal incidence is zero. Highly resonant coupling between the plane wave and the Bloch mode occurs only around normal incidence. In contrast, the bright mode couples to the plane wave under normal incidence, leading to a resonant interaction.

It is also noticeable that, in the vicinity of normal incidence, in the direction of the closest reciprocal lattice vector neighbors ( $\Gamma X$  direction), the bands can be more or less flat, leading to possible robustness of the modes at oblique incidence.

In addition to the band diagrams, electromagnetic field maps can help identifying the modes involved in light trapping. As mentioned previously, field maps in the ( $x, y$ ) space can indicate the dark or bright nature thanks to their symmetry [12], whereas their main spatial harmonic reveals the diffractive order still according to the band folding. Additionally,  $E_y(y, z)$  or  $H_y(y, z)$  maps allow the identification of the guided modes implied in the diffraction process. These components never cancel along the  $z$ -direction for the fundamental guided modes, whereas they cancel once for the first order guided mode.

Moreover, the enhancement of absorptance by a Bloch resonance has been established [17]. In the basic case of a structure having a ( $x, y$ ) symmetry plane, a 50% peak absorptance could be reached owing to a single Bloch resonance under the so-called “critical coupling conditions”. The quality factor is then evaluated by:

$$Q = \frac{n}{2\kappa}, \quad (6)$$

where  $n$  and  $\kappa$  are the refractive index and the extinction coefficient of the material, respectively. Given the  $\text{TiO}_2$  considered here and its dispersion, the expected  $Q$  can be as low as 10 at the shortest wavelength of the spectral domain of interest. It increases drastically as,  $\kappa$  tends to zero (thus  $Q$  to infinity) when  $\text{TiO}_2$  is at its band edge. In the cases of an asymmetric device and spectral overlap of at least two modes, the absorptance can surpass 50% [18]. In our case, numerous bright modes, resulting from the mechanisms previously discussed, can possibly exist in a limited spectral range (few tens of nm). Thus, all these modes can contribute to enhance the absorptance of a low absorbing material within the PC membrane. Even “dark modes” could contribute to this enhancement, but at slightly oblique incidence, making these structures even more robust to the angle of incidence of the light.

### 3. Simulation results and discussion

The spectral absorptance of all the structures with parameters in the ranges shown in **Tab. 1** have been rigorously calculated, as well as the one of the corresponding planar references with the same thickness  $t$ . The resulting enhancement factor values  $\xi$  are presented in the following. For the pillar and hole structures exhibiting the largest  $\xi$ , a modal analysis enables a deep understanding of the LT mechanism and leads to some guidelines.

### 3.1. Absorptance of planar references

The absorptance spectra of planar stacks have been calculated for various  $t$ . **Figure 2** shows that the absorptance in TiO<sub>2</sub> is weakly dependent on  $t$  and is overall limited in this spectral range.

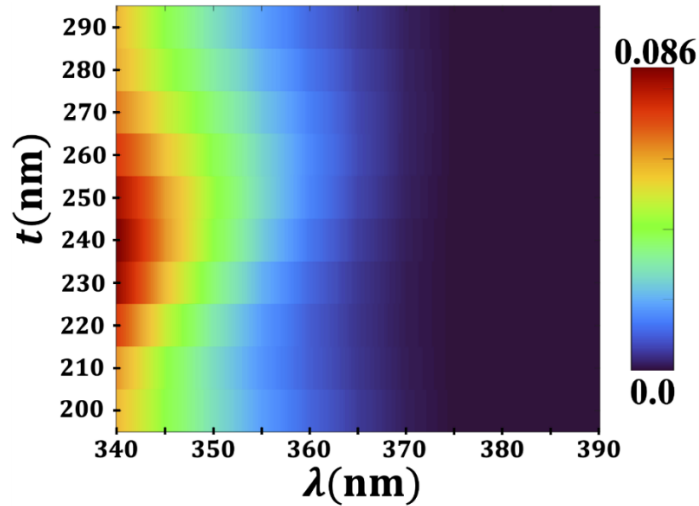


**Fig. 2.** Absorptance spectra of planar references for thickness values  $t$  in the range [200–290 nm].

The derived integrated absorptance per unit area  $A_{int.ref}$  will be used as a reference for the enhancement factor ( $\xi$ ) calculation for the various envisaged parameters.

### 3.2. Integrated absorptance enhancements

**Figure 3** summarizes the best enhancements  $\xi$  as a function of  $t$  and  $H$  (for each couple of these values, the  $P$  and  $aff$  leading to the largest  $\xi$  were chosen), for holes (left) and pillars (right), over the [340–375 nm] spectral range.

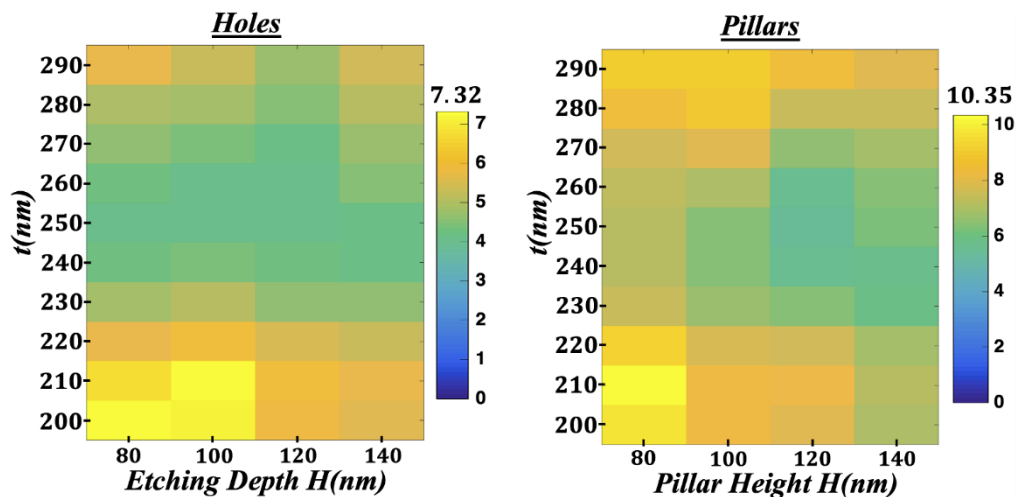
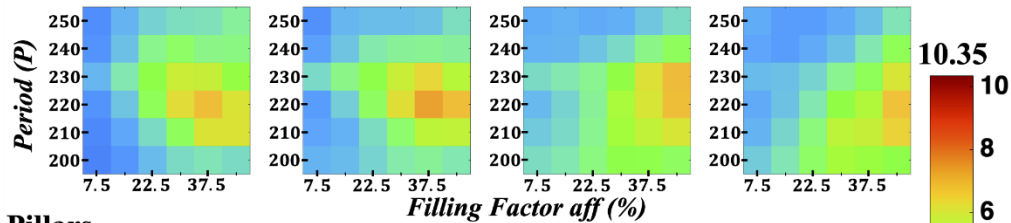


**Fig. 3.** Enhancement of the integrated absorptance obtained with backbone made of holes (left) and pillars (right), in the [340–375 nm] spectral range.

It clearly appears an optimum of  $t$ , among the thinnest of the envisaged range, whereas the optimum of  $H$  remains lower than half of  $t$ . It is also noticeable that structures with pillars offer a better enhancement ( $\xi = 10.35$ ) compared to those with holes ( $\xi = 7.32$ ).

**Figure 4** shows detailed enhancement  $\xi$  for holes and pillars as a function of  $aff$ , and  $H$  for the best  $t$  for both structures, i.e.  $t = 210$  nm. For holes,  $\xi = 7.32$  is obtained with  $P = 220$  nm and  $aff = 37.5\%$ . For pillars,  $\xi = 10.35$  is obtained with  $P = 220$  nm and  $aff = 80\%$ .

### Holes



### Pillars

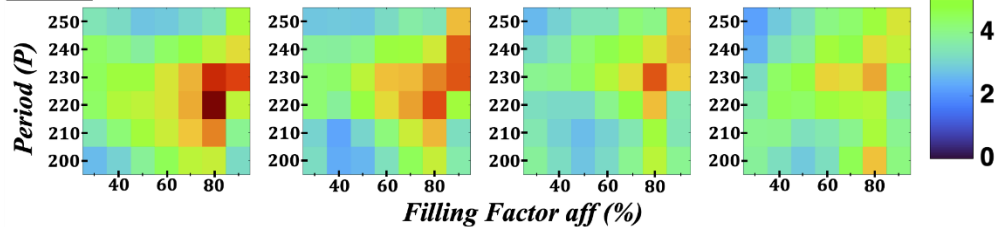


**Fig. 4.** Enhancement of the integrated absorbance with backbone made of holes (left) and pillars (right) structure, in spectral range [340–375 nm], for  $t = 210$  nm for both holes and pillars.

These resonances can be clearly observed in the corresponding absorbance spectra in **Fig. 5**. The integrated absorbance is considerably larger than the one of the flat reference (14.55 times larger for holes, and 16.32 times for pillars), although but it should be noted that the surface of  $\text{TiO}_2$  is also larger. It can be noticed that, without weighting by the volume of  $\text{TiO}_2$ , the quality factor calculated in Eq. (6) for the involved modes is exactly in the range deriving from the simple case of a homogenous membrane in the range [340–360 nm], since highly resonant modes at larger wavelengths would not significantly contribute to  $\xi$ . Moreover, the absorbance overpasses 50% due to the contribution of several modes, as detailed below, and the asymmetry of the device. Finally, as can be seen in **Fig. 5**, the transmittance of both samples is significantly larger than that of the planar reference, over the visible range, except at two rather sharp resonances in the blue as detailed in the following.

### 3.3. Band diagram analysis

**Figure 6** presents the angle-resolved simulated reflectance (on the top) and absorbance (on the bottom) maps, for both polarizations of the incident light (i.e. S polarization (left panel) and P polarization (right panel)). Along the  $\Gamma X$  direction corresponding to the angular scanning in simulations, S polarization stands for  $(E_y, H_x, H_z)$  and P for  $(H_y, E_x, E_z)$  in the far field. The angle of incidence is swept in the range  $[-20^\circ, 20^\circ]$ , whereas the wavelength range is [340 - 440 nm]. These maps can be regarded as partial band diagrams of the structures. Finally, it is worth reminding that S and P states are equivalent at the  $\Gamma$  point, meaning that both diagrams correspond to the spectra in **Fig. 5**.

Given the investigated range of periods, the lowest Bloch resonances occur at the shortest wavelength of the visible range. At larger wavelengths, the PC simply acts as a medium of

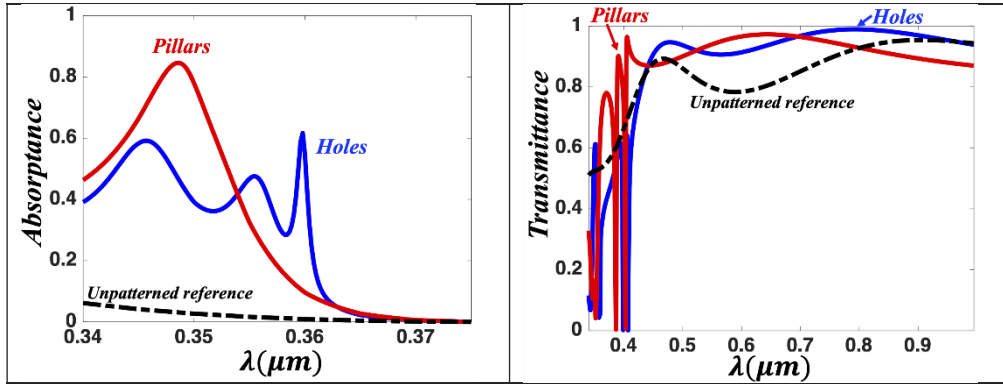


**Fig. 5.** : Absorbance spectra (left) and Transmittance spectra, including the visible region, (right), for structures leading to the best enhancement factor, either with holes ( $t = 210$  nm,  $P = 220$  nm,  $aff = 37.5\%$ ,  $H = 100$  nm) or pillars ( $t = 210$  nm,  $P = 220$  nm,  $aff = 80\%$ ,  $H = 80$  nm). Spectra of unpatterned reference are shown for comparison.

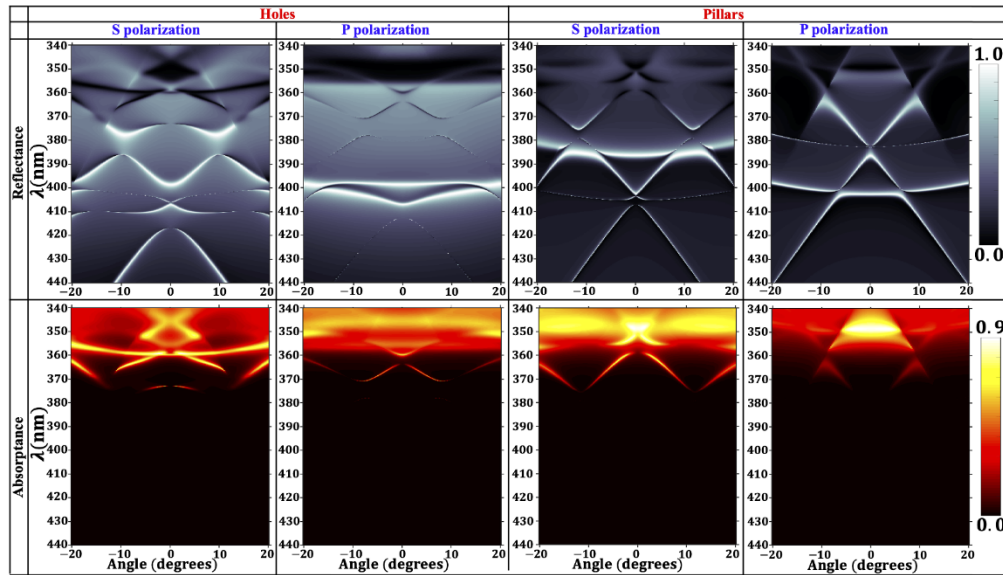


**Fig. 6.** Angle resolved simulated reflectance (top) and absorbance (bottom) maps, for S polarization of incident wave and P polarization, for structures with holes (left) and pillars (right).

average index between air and  $\text{SiN}_x$ , thus reducing the reflectance when compared to the flat reference, as shown in **Fig. 5(b)**.

In the region of  $\text{TiO}_2$  transparency, Bloch resonances correspond to high reflectance, whereas in the region of  $\text{TiO}_2$  absorption, Bloch resonances lead to large absorptance. Physically, the dark modes cannot be excited under normal incidence. However, provided they are highly resonant and rather far from the modes, they remain easy to identify, thanks to their reflectance or absorptance tending to zero around the normal incidence.

The properties discussed in section 2.3 are used to identify the Bloch resonances in these diagrams. It turns out that the four lowest energy modes, for each polarisation state on the partial band diagrams of the structures, in the transparency region, mainly correspond to the first diffraction order of the fundamental TE and TM guided modes. A first proof-of-concept is given by the bandfolding mechanism (see an illustration of these mechanisms in **Fig. S3**); whereas a second proof of concept is obtained thanks to the electro-magnetic fields maps (see **Fig. S4**). Indeed, the  $E_y$  spatial profile of the S-polarized Bloch resonances (respectively  $H_y$  of the P modes) should not exhibit any node (i.e. zero value) along  $z$ , as discussed in section 2.3, even if possible mode coupling could affect the profiles. Moreover, the in-plane  $E_x$  and  $E_y$  profiles of the various modes should exhibit only one period over the unit cell, with symmetry properties satisfying the “dark” and “bright” Bloch resonances, and thus follow the typical profiles of the first diffracted order in a 2D square lattice (see details in **Fig. S5**).

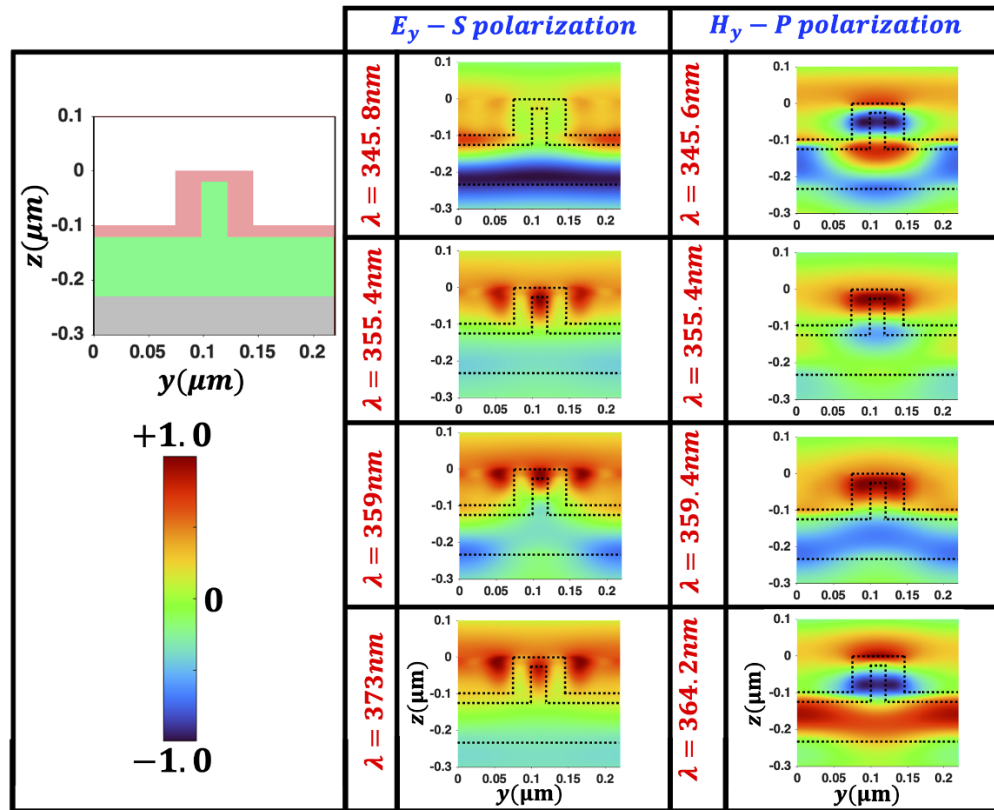


**Fig. 7.** Backbone with holes.  $E_y$  profiles of the S Bloch resonances (left) and  $H_y$  profiles of the P Bloch resonances (right) implied in the absorption enhancement. Angle of incidence is equal to 1 degree.

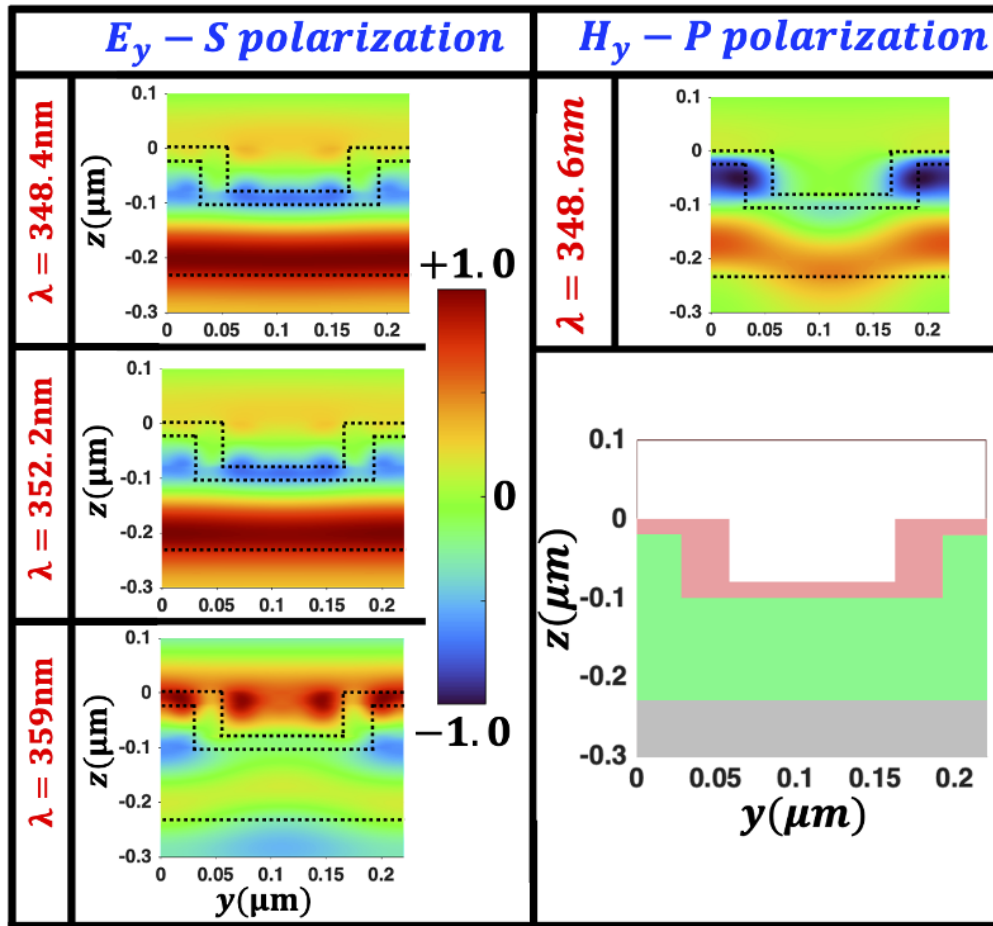


**Fig. 8.** Backbone with pillars -  $E_y$  profiles of the S Bloch resonances (left) and  $H_y$  vertical profiles of the P Bloch resonances (right) implied in the absorption enhancement. Angle of incidence is equal to 1 degree.

However, such Bloch resonances with antinodes (i.e. extremum values), close to the middle plane along the vertical profile of the structure, show less overlapping with the active material close to the surface, and therefore less absorptance enhancement.

In the absorption region, the Bloch resonances, responsible for the largest  $\xi$ , stem from higher order guided modes, in line with the band folding mechanism (see **Fig. S3**). It is also confirmed by examining the field maps at selected wavelengths (**Fig. 7 and 8**) where at least one node is present over the vertical profile, as well as antinodes that have better chance to overlap the active material, leading to a better absorption in the  $\text{TiO}_2$  layer conformally deposit on  $\text{SiN}_x$ .

All these considerations explain the existence of an optimal thickness  $t$  for both structures, such as the  $m = 1$  guided modes of the unpatterned stack are close to their cut-off (similar mode solving as those used for Table S1 lead to  $n_{\text{eff } TE,1} = 1.598$  and  $n_{\text{eff } TM,1} = 1.523$  at  $\lambda = 360$  nm). For thicknesses larger than the optimal one, these Bloch resonances are redshifted outside the absorption region due to their larger effective index. The higher order diffracted modes that could exist in this spectral range lead to a lower absorption.

Thus, the optimal period  $P = 220$  nm is in line with the value derived from the grating law at the first diffraction order ( $P = \frac{\lambda}{n_{eff,1}} \approx 230$  nm provided  $n_{eff,1} \sim 1.56$  as an approximate value independent of the polarization state, at  $\lambda = 360$  nm)

Finally, the dispersion properties show that the partial degeneracy of several of these modes advantageously contributes to the large absorptance, especially in the case of pillars. This seems likely to be the main reason of the larger  $\xi$  compared to the structure with holes.

We conducted another simulation to estimate the impact of water, which could partly replace air at the vicinity of the sample. Regardless of wettability considerations, it is simply assumed here that water (refractive index from [19]) completely replaces air, and is thus considered as the incidence medium in the simulation. For both holes and pillars, the absorptance appears to be robust to the change of refractive index in the medium of incidence (see Fig. 9).

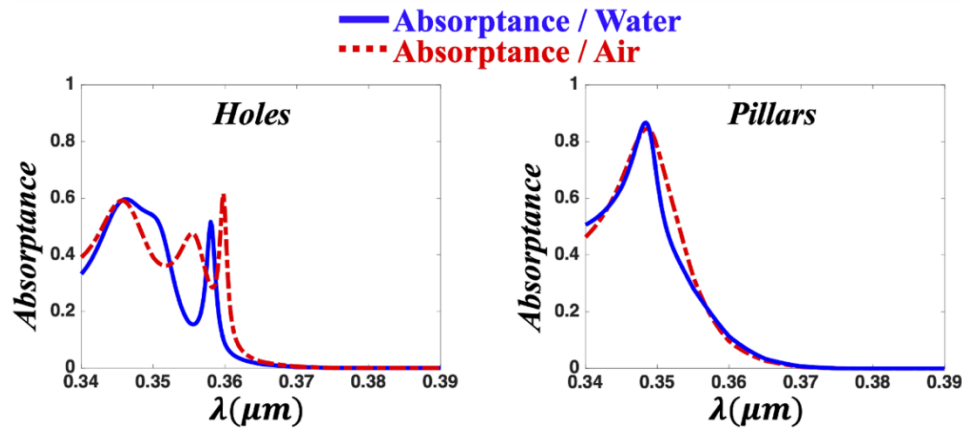


**Fig. 9.** : Comparison of the absorption spectra using water or air as incidence medium for the structure with holes ( $t = 210$  nm,  $P = 220$  nm,  $aff = 37.5\%$ ,  $H = 100$  nm, on the left) and pillars ( $t = 210$  nm,  $P = 220$  nm,  $aff = 80\%$ ,  $H = 80$  nm, on the right).

### 3.4. Summary and guidelines

In summary, transparent  $\text{SiN}_x$  backbones, thick enough to act as multimode waveguides, are only partially etched and so easier to fabricate, with a period still achievable with UV lithography (see below). Interestingly, these structures are shown to drastically enhance the normalized integrated absorptance of  $\text{TiO}_2$  (more than 16 times) within the same footprint compared to a flat sample, and up to more than 10 times for a same volume of  $\text{TiO}_2$ , mainly due to a LT effect. Moreover, phenomenological mechanisms can help targeting the proper range of parameters, namely the thickness and the period of the backbone.

## 4. Fabrication and optical measurement of a demonstrator

In order to validate the technical feasibility of such samples on large surfaces (i.e.  $\sim 4$  cm<sup>2</sup> see Fig. 10) using rather low cost and versatile techniques, the optical properties have been checked on a structure made of holes.

A 200-nm thick  $\text{SiN}_x$  layer is deposited on a glass substrate by plasma enhanced chemical vapor deposition (PECVD). A negative photoresist coating is patterned by interference lithography at the wavelength of 266 nm. The pattern is transferred into  $\text{SiN}_x$  using Reactive Ion Etching plasma, with an etch depth of  $H = 100$  nm. The 20 nm thick  $\text{TiO}_2$  layer is finally deposited by ALD.



**Fig. 10.** Views of samples at grazing incidence (on the left, the green color can be related to the diffraction of the Bloch mode in S polarization that exists at large wavelengths for such patterns and that is partly visible in Fig. 7 and Fig. 11) and under normal incidence (in the middle, the sample is transparent). SEM image of one the fabricated sample (on the right).

The SEM image (**Fig. 10(b)**) of a fabricated sample was used to determine the average values  $P = 224$  nm and  $aff = 32.4\%$ .

The fabricated structure was experimentally characterized to obtain the partial band structure by performing angle-resolved reflectance measurements. Back Focal Plane imaging [20] was used, mainly in the transparency region [360–440 nm] (limited by the optics of the setup), along the  $\Gamma X$  direction, for both S and P polarized incident light.

Experimental reflectance measurements are compared to RCWA simulation using experimentally determined parameters above (**Fig. 11**). Both band structures show a rather good agreement, especially for the highly reflective, broader bands. Since the theoretical band diagram is also close the one presented in **Fig. 7** for the theoretically optimized structure, such a sample constitutes a proof-of-concept of the technical feasibility of samples enabling an absorption enhancement at the scale of a few centimetre square.

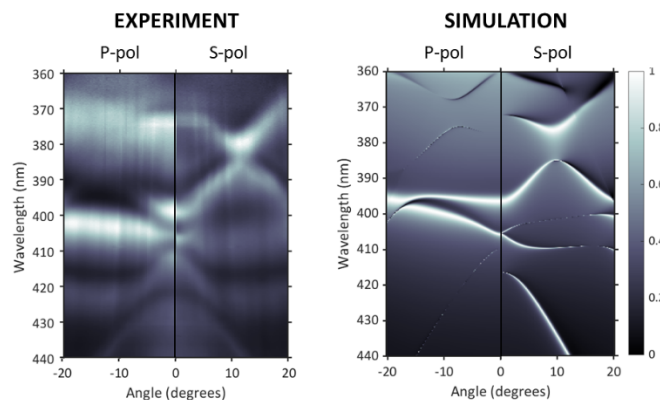


**Fig. 11.** : (a) Experimental measurements, (b) Angle-resolved simulated reflectance map for S and P-polarized light.

Practically, such devices have shown an enhancement in the UV photocatalysis efficiency correlated with absorption enhancements resulting from the patterning, especially in the case of the NO oxidation reaction [21].

## 5. Conclusion

The optical properties of structures consisting of a transparent  $\text{SiN}_x$  matrix patterned as a PC with cylindrical air holes or pillars covered by an ultrathin absorbing layer have been investigated.

Using a 20 nm thick conformally deposited TiO<sub>2</sub> active layer is considered as a case study for applications in the field of photocatalysis, relying on photon absorption in the near UV range while the structure is highly transparent over the visible range.

RCWA method has been used to calculate both spectra and band dispersion. By adjusting the geometrical parameters, we have identified photonic structures leading to the highest integrated absorbance enhancement, normalized by the surface ratio, compared to the unpatterned structure. An in-depth optical mode analysis has revealed that the Bloch resonances arising from the highest order guided modes are responsible for the optimized absorption.

As an illustration of this approach, and to confirm its feasibility, a few centimeter square bilayer PC was fabricated and characterized. Results showed a good agreement with numerical simulations, suggesting that scalable processes, compatible with low-cost production can be used to reach high efficiency absorption on ultrathin layers typical structures.

This work paves the way to efficient PC, mostly transparent in the visible domain, and highly absorbing in the UV. Such structures are expected to be useful, for air or water depollution, as well as solar energy conversion to solar fuels such as in the case of water splitting or artificial photosynthesis. Owing to their transparency at larger wavelengths, their association with other solar energy converters, such as photovoltaic modules, could be envisaged for an optimized use of the solar irradiation.

**Funding.** Agence Nationale de la Recherche (ANR-16-IDEX-0005).

**Acknowledgement.** RCWA simulations were performed on Nanolyon cluster facility as well as on the Newton computer cluster facilities operated by PMCS2I at Ecole Centrale de Lyon. The samples were fabricated and measured in the Nanolyon platform.

**Disclosures.** The authors declare no conflicts of interest.

**Data availability.** Data underlying the results presented in this paper are not publicly available at this time but may be obtained from the authors upon reasonable request.

**Supplemental document.** See [Supplement 1](#) for supporting content.

## References

1. H.-L. Chen, A. Cattoni, R. D. Lépinau, A. W. Walker, O. Höhn, D. Lackner, G. Siefert, M. Faustini, N. Vandamme, J. Goffard, B. Behaghel, C. Dupuis, N. Bardou, F. Dimroth, and S. Collin, "A 19.9%-efficient ultrathin solar cell based on a 205-nm-thick GaAs absorber and a silver nanostructured back mirror," *Nat. Energy* **4**(9), 761–767 (2019).
2. J. Liu, H. Zhao, M. Wu, B. Van der Schueren, Y. Li, O. Deparis, J. Ye, G. A. Ozin, T. Hasan, and B.-L. Su, "Slow Photons for Photocatalysis and Photovoltaics," *Adv. Mater.* **29**(17), 1605349 (2017).
3. X. Zhang and S. John, "Photonic crystal based photoelectrochemical cell for solar fuels," *Nano Select* **2**(6), 1218–1224 (2021).
4. O. Deparis, S. R. Mouchet, and B.-L. Su, "Light harvesting in photonic crystals revisited: why do slow photons at the blue edge enhance absorption?" *Phys. Chem. Chem. Phys.* **17**(45), 30525–30532 (2015).
5. X. Zhang and S. John, "Enhanced photocatalysis by light-trapping optimization in inverse opals," *J. Mater. Chem. A* **8**, 18974–18986 (2020).
6. H. Chang, K. Min, M. Lee, M. Kang, Y. Park, K.-S. Cho, Y.-G. Roh, S. W. Hwang, and H. Jeon, "Colloidal quantum dot lasers built on a passive two-dimensional photonic crystal backbone," *Nanoscale* **8**(12), 6571–6576 (2016).
7. N.-V. Hoang, A. Pereira, H. S. Nguyen, E. Drouard, B. Moine, T. Deschamps, R. Orobtcchouk, A. Pillonnet, and C. Seassal, "Giant Enhancement of Luminescence Down-Shifting by a Doubly Resonant Rare-Earth-Doped Photonic Metastructure," *ACS Photonics* **4**(7), 1705–1712 (2017).
8. C. Gong, W. Liu, N. He, H. Dong, Y. Jin, and S. He, "Upconversion enhancement by a dual-resonance all-dielectric metasurface," *Nanoscale* **11**(4), 1856–1862 (2019).
9. C. Würth, P. Manley, R. Voigt, D. Ahiboz, C. Becker, and U. Resch-Genger, "Metasurface Enhanced Sensitized Photon Upconversion: Toward Highly Efficient Low Power Upconversion Applications and Nanoscale E-Field Sensors," *Nano Lett.* **20**(9), 6682–6689 (2020).
10. D. T. Vu, Y.-C. Tsai, Q. M. Le, S.-W. Kuo, N. D. Lai, H. Benisty, J.-Y. Lin, H.-C. Kan, and C.-C. Hsu, "A Synergy Approach to Enhance Upconversion Luminescence Emission of Rare Earth Nanophosphors with Million-Fold Enhancement Factor," *Crystals* **11**(10), 1187 (2021).
11. A. Fujishima and K. Honda, "Electrochemical Photolysis of Water at a Semiconductor Electrode," *Nature* **238**(5358), 37–38 (1972).

12. L. Lu, Q. Le-Van, L. Ferrier, E. Drouard, C. Seassal, and H. S. Nguyen, "Engineering a light-matter strong coupling regime in perovskite-based plasmonic metasurface: quasi-bound state in the continuum and exceptional points," *Photonics Res.* **8**(12), A91 (2020).
13. M. G. Moharam and T. K. Gaylord, "Rigorous coupled-wave analysis of planar-grating diffraction," *J. Opt. Soc. Am.* **71**(7), 811–818 (1981).
14. V. Liu and S. Fan, "S4: A free electromagnetic solver for layered periodic structures," *Comput. Phys. Commun.* **183**(10), 2233–2244 (2012).
15. M. L. Brongersma, Y. Cui, and S. Fan, "Light management for photovoltaics using high-index nanostructures," *Nat. Mater.* **13**(5), 451–460 (2014).
16. J.-M. Lourtioz, ed., *Photonic Crystals: Towards Nanoscale Photonic Devices* (Springer, 2005).
17. Y. Park, E. Drouard, O. E. Daif, X. Letartre, P. Viktorovitch, A. Fave, A. Kaminski, M. Lemiti, and C. Seassal, "Absorption enhancement using photonic crystals for silicon thin film solar cells," *Opt. Express* **17**(16), 14312–14321 (2009).
18. R. Peretti, G. Gomard, C. Seassal, X. Letartre, and E. Drouard, "Modal approach for tailoring the absorption in a photonic crystal membrane," *J. Appl. Phys.* **111**(12), 123114 (2012).
19. M. Daimon and A. Masumura, "Measurement of the refractive index of distilled water from the near-infrared region to the ultraviolet region," *Appl. Opt.* **46**(18), 3811–3820 (2007).
20. R. Wagner, L. Heerklotz, N. Kortenbruck, and F. Cichos, "Back focal plane imaging spectroscopy of photonic crystals," *Appl. Phys. Lett.* **101**(8), 081904 (2012).
21. J. Capitolis, M. Hamandi, M. Hochedel, S. El-Jallal, E. Drouard, C. Chevalier, J.-L. Leclercq, J. Penuelas, T. Dursap, S. Brottet, B. Devif, H. S. Nguyen, G. Berhault, J.-M. Chovelon, C. Ferronato, C. Guillard, E. Puzenat, N. Crespo-Monteiro, S. Reynaud, Y. Jourlin, M. Bugnet, and C. Seassal, "Two-dimensional photonic metasurfaces for slow light-controlled photocatalysis," *Nano Select* **3**(1), 108–117 (2022).